IJMMM International Journal of Minerals, Metallurgy and Materials 矿物冶金与材料学报（英文版）

MgO-attached graphene nanosheet (MgO@GNS) reinforced magnesium matrix nanocomposite with superior mechanical, corrosion and biological performance

S. Abazari, A. Shamsipur, H.R. Bakhsheshi-Rad, M.S. Soheilirad, F. Khorashadizade, and S.S. Mirhosseini

Cite this article as:
S. Abazari, A. Shamsipur, H.R. Bakhsheshi-Rad, M.S. Soheilirad, F. Khorashadizade, and S.S. Mirhosseini, MgO-attached graphene nanosheet (MgO@GNS) reinforced magnesium matrix nanocomposite with superior mechanical, corrosion and biological performance, *Int. J. Miner. Metall. Mater.*, 31(2024), No. 9, pp. 2062-2076. https://doi.org/10.1007/s12613-023-2797-0

Articles you may be interested in

Mahmood Razzaghi, Masoud Kasiri-Asgarani, Hamid Reza Bakhsheshi-Rad, and Hamid Ghayour, *In vitro* bioactivity and corrosion of PLGA/hardystonite composite-coated magnesium-based nanocomposite for implant applications, *Int. J. Miner. Metall. Mater.*, 28(2021), No. 1, pp. 168-178. https://doi.org/10.1007/s12613-020-2072-6

Jin-long Su, Jie Teng, Zi-li Xu, and Yuan Li, Biodegradable magnesium-matrix composites: A review, *Int. J. Miner. Metall. Mater.*, 27(2020), No. 6, pp. 724-744. https://doi.org/10.1007/s12613-020-1987-2

Muharrem Pul, Effect of sintering temperature on pore ratio and mechanical properties of composite structure in nano graphene reinforced ZA27 based composites, *Int. J. Miner. Metall. Mater.*, 27(2020), No. 2, pp. 232-243. https://doi.org/10.1007/s12613-019-1926-2

Yong Mei, Pu-zhen Shao, Ming Sun, Guo-qin Chen, Murid Hussain, Feng-lei Huang, Qiang Zhang, Xiao-sa Gao, Yin-yin Pei, Su-juan Zhong, and Gao-hui Wu, Deformation treatment and microstructure of graphene-reinforced metalmatrix nanocomposites: A review of graphene post-dispersion, *Int. J. Miner. Metall. Mater.*, 27(2020), No. 7, pp. 888-899. https://doi.org/10.1007/s12613-020-2048-6

Shang-hao Tong, Yong Li, Ming-wei Yan, Peng Jiang, Jia-jia Ma, and Dan-dan Yue, *In situ* reaction mechanism of MgAlON in Al-Al_2O_3-MgO composites at 1700 under flowing N_2, *Int. J. Miner. Metall. Mater.*, 24(2017), No. 9, pp. 1061-1066. https://doi.org/10.1007/s12613-017-1496-0

Akhya kumar Behera, Amlan Das, Sanjeev Das, and Archana Mallik, Electrochemically functionalized graphene as an anti-corrosion reinforcement in Cu matrix composite thin films, *Int. J. Miner. Metall. Mater.*, 28(2021), No. 9, pp. 1525-1533. https://doi.org/10.1007/s12613-020-2124-y

IJMMM WeChat

QQ author group

INTERNATIONAL JOURNAL OF
Minerals, Metallurgy and Materials

Volume 31, Number 9, September 2024
Page 2062

Research Article https://doi.org/10.1007/s12613-023-2797-0

MgO-attached graphene nanosheet (MgO@GNS) reinforced magnesium matrix nanocomposite with superior mechanical, corrosion and biological performance

S. Abazari[1,2], *A. Shamsipur*[1)✉], *H.R. Bakhsheshi-Rad*[3)✉], *M.S. Soheilirad*[2)], *F. Khorashadizade*[4)], *and S.S. Mirhosseini*[1)]

1) Department of Materials and Metallurgical Engineering, Amirkabir University of Technology, Tehran 1599637111, Iran
2) Iranian National Standards Organization of Hormozgan, Hormozgan, Iran
3) Advanced Materials Research Center, Department of Materials Engineering, Najafabad Branch, Islamic Azad University, Najafabad, Iran
4) Department of Materials and Metallurgical Engineering, Iran University of Science and Technology, Tehran, Iran
(Received: 23 May 2023; revised: 21 July 2023; accepted: 10 October 2023)

Abstract: Magnesium (Mg) alloys are gaining great consideration as body implant materials due to their high biodegradability and biocompatibility. However, they suffer from low corrosion resistance and antibacterial activity. In this research, semi-powder metallurgy followed by hot extrusion was utilized to produce the magnesium oxide@graphene nanosheets/magnesium (MgO@GNS/Mg) composite to improve mechanical, corrosion and cytocompatibility characteristics. Investigations have revealed that the incorporation of MgO@GNS nanohybrids into Mg-based composite enhanced microhardness and compressive strength. In vitro, osteoblast cell culture tests show that using MgO@GNS nanohybrid fillers enhances osteoblast adhesion and apatite mineralization. The presence of MgO@GNS nanoparticles in the composites decreased the opening defects, micro-cracks and micro-pores of the composites thus preventing the penetration of the corrosive solution into the matrix. Studies demonstrated that the MgO@GNS/Mg composite possesses excellent antibacterial properties because of the combination of the release of MgO and physical damage to bacterium membranes caused by the sharp edges of graphene nanosheets that can effectively damage the cell wall thereby facilitating penetration into the bacterial lipid bilayer. Therefore, the MgO@GNS/Mg composite with high mechanical strength, antibacterial activity and corrosion resistance is considered to be a promising material for load-bearing implant applications.

Keywords: metal matrix composites; MgO@GNS nanohybrid; strengthening mechanisms; antibacterial activity; biocompatibility

1. Introduction

Magnesium (Mg) has obtained much attention for developing biodegradable fracture repair systems due to its strong resemblance to the bone in terms of Young's modulus and density. Mg is the fourth most abundant cation in the body and its degradation is tolerated by body tissue very well, as evidenced by several animal experiments [1–4]. However, Mg has a high corrosion rate, causing the fast release of hydrogen gas and a quick degradation rate, which causes a reduction of mechanical strength [5–8]. Thus, implant failure has been a big concern to their broad use [9]. As a result, it is important to produce Mg matrix materials with improved mechanical characteristics with a low corrosion rate [10]. Recent research has been carried out to lower the degradation rate of Mg using alloying and powder metallurgy for the preparation of composite [9–12]. Mg ions have also been demonstrated to be essential for endothelial cell growth and activity, as well as to have modest antiarrhythmic and thrombogenic characteristics, which may limit platelet activation on the surface and abnormal microvessel contraction [13]. Mg has an intrinsic antibacterial property via a photothermal mechanism that produces localized heat, preventing bacterial invasion. As a result, Mg is an excellent material for improving the mechanical and biological properties of polylactic acid (PLA) composites, as well as imparting antibacterial qualities [14].

Mg–Zn alloy has lately attracted a lot of interest since Zn is necessary for the body and has high biocompatibility [15]. Metal matrix composites (MMCs) prepared with nano reinforcements are regarded as an attractive model for improving both mechanical and corrosion characteristics of Mg-based biocomposite for load bearing usages [13–14]. According to reports, nanofillers have been extensively utilized as reinforcing agents to boost the mechanical characteristics of Mg matrix composites [16–18]. In this study, graphene

✉ Corresponding authors: A. Shamsipur E-mail: shamsipur@aut.ac.ir;
H.R. Bakhsheshi-Rad reza.bakhsheshi@gmail.com, rezabakhsheshi@pmt.iaun.ac.ir

nanosheets (GNS) and MgO nanoparticles as hybrid fillers were incorporated together to form a composite structure; in this structure spherical MgO nanoparticles were attached to the surface of the GNS. The combination nanostructure was incorporated into the Mg-based matrix to increase dispersion and increase the composite efficiency for load bearing medical purposes [17,19]. MgO as a nano-additive have antibacterial properties and is one of the primary constituents of bioglass with outstanding thermal and mechanical properties. Furthermore, MgO is fully degradable in vivo, yielding the same compounds as Mg [20]. According to Goh *et al.* [21], the incorporation of MgO nanoparticles into Mg-based composites enhanced their microhardness, yield, and tensile strength. The major cause for this enhancement is to be minor, intrinsic defects in MgO nanoparticles and excellent MgO/Mg interfacial bonding. Furthermore, Lei *et al.* [12] found that the incorporation of MgO reinforcement to the Mg matrix improved the corrosion behavior and mechanical characteristics of the composite using an *in-situ* reaction sintering process [22]. Some methods have been investigated to enhance the biological, mechanical, and corrosion characteristics of materials based on Mg with the addition of a two-dimensional (2D) nano reinforcement [23].

In recent years, graphene nanosheets (GNS), 2D material, have attracted the attention of researchers due to their good mechanical, chemical and physical characteristics [24–26]. GNS and its derivatives have been considered promising building blocks in functional Mg-based composites due to their unique comprehensive properties and their ability to be mass production [27–28]. Hot working also is a process of enhancing mechanical characteristics through rolling or extrusion because of their function in dynamic recrystallization [29]. In this respect, it was reported [30] that hot extrusion is utilized to modify the densification of composites since it is hard to avoid micropore production in composites after sintering. Therefore, graphene sheets attached with MgO are used to develop Mg matrix composites with increased strength without decreasing toughness, with appropriate corrosion behavior and biological properties [31]. GNS and graphene oxide (GO) are significantly resistant to corrosive medium penetration. They can function as a barrier, because of the density of their layers which results from the actual sp^2 hexagonal structure of carbon atoms [32]. The inertness and stability of GO and RGO sheets are reported as important aspects, providing them with appropriate reinforcements for enhancing the anti-corrosion of coating properties [33]. Also, recent research has demonstrated that GO is an extremely efficient antibacterial additive against two different pathogenic bacteria. Additionally, it was reported that the charge transfer among bacterial cells and GO is the cause of this antibacterial activity [34]. Ball milling is a complex method that requires the tuning of several factors in order to get the desired results. In addition, it generates heat that can easily burn magnesium powder. As a result, solution-based powder metallurgy is used to create the GNPs/multi-walled carbon nanotubes (MWCNTs)-based Mg composites [35–36].

However, homogeneous dispersion of graphene sheets in Mg composites is difficult because of their poor wettability by molten Mg and tends to cluster due to the large specific surface [37]. As a result, in addition to the low strength efficiency of GNS, strengthening is often accompanied by less fracture strain [38–39]. To develop the homogeneous distribution of graphene, nano-additives such as MgO were applied by researchers. Several studies [20,40–42] have shown that MgO can grow directly on graphene and that its interfacial bonding properties are enhanced by the presence of strong carbon–oxygen bonds. Because of its excellent lattice match, MgO can develop stronger interfacial bonding with the Mg Metal matrix [42–43]. In another study, MgO@carbon nanotube (CNT)-reinforced AZ91 alloy composites were developed by Yuan *et al.* [44]. In their work, MgO was added to CNTs to improve the interfacial bonding between CNT reinforcement and the Mg. Nevertheless, because of CNTs tend to self-assemble into clusters, the required level of dispersion was not reached [45]. So far, few studies have been reported on the effect of MgO on the GNS tending to self-assemble into clusters and the influence of biodegradation protection of GNS for Mg alloys. Hence, in this study, MgO@GNS nanohybrid reinforced Mg–3Zn alloy composites were fabricated via semi powder metallurgy (SPM) followed by hot extrusion method to decrease the degradation rate and improve mechanical properties and biological properties.

2. Experimental

2.1. Materials

Pure Mg powder (99.8% purity, 50 μm mean particle size) and Zn powder (size 98.8% purity, 7.5 μm mean particle) supplied by Sigma-Aldrich Co., Ltd., USA were used as the raw materials. GNS (thickness of 2 nm and plane size of 1–10 μm mean) was also purchased from US-nano Co. as the initial reinforcing agent. The MgO covered GNS termed MgO@GNS (nanohybrid reinforcement) was created utilizing a chemical coating method [46].

2.2. Preparation of MgO@GNS/Mg composites

The Mg and Zn powders were milled under the argon gas at 300 r/min for 25 h to produce Mg–3Zn alloy powder via the planetary ball mill. According to Ref. [42], magnesium oxide (MgO) nanoparticles are coated on reduced graphene oxide (RGO) surface and then introduced in AZ61 alloy by laser melting, expecting to strengthen the interfacial bonding between Mg matrix and RGO. The findings show that MgO functions as an interfacial bridge between the Mg matrix and RGO, developing nanoscale contact and distortion areas with RGO. GNS was first oxidized using a mixture of strong sulfuric acid and nitric acid to remove impurities and obtain carboxylic acid groups on the surface of carbon nanomaterial [47]. Due to chelating, the carboxylic acid groups have significant contact with metal ions, allowing metal ions to be absorbed on the surface of GNS. After adding ammonia, Mg^{2+} ions were converted into insoluble $Mg(OH)_2$ and sub-

sequently calcined to MgO coated on the surface of GNS. Then MgO@GNS powders were added to ethanol for 2 h using an ultrasonic bath. Subsequently, suspension of MgO@GNS and Mg were combined and agitated for 1 h mechanically to produce MgO@GNS/Mg nanocomposite mixtures, then were filtered and dried in vacuum at 343 K for 24 h to provide the MgO@GNS/Mg nanocomposite powders. Under 120 MPa hydraulic pressure, the composite powders were pressed in a cylinder mold that was 200 mm in height and 40 mm in diameter. Consequently, the samples were sintered in an Ar gas environment in a tube furnace for 2 h at 873 K. The homogeneous billets were hot extruded with 11:1 extrusion ratio at 673 K (as shown in Fig. 1). Also by using the same techniques, the Mg-based alloy and the related GNS/Mg composites were fabricated (compacting, sintering, and hot extrusion).

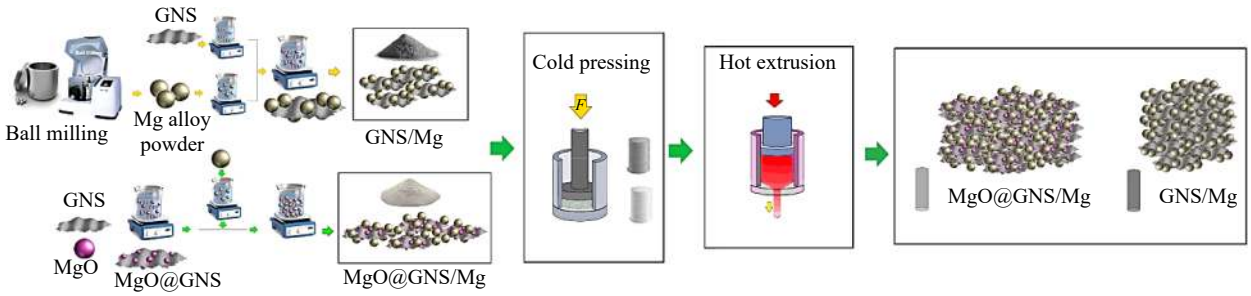

Fig. 1. Scheme of the synthesis procedure for GNS/Mg and MgO@GNS/Mg nanocomposites.

2.3. Characterization

To evaluate the microstructure and phase component of samples, X-ray diffraction (XRD, Siemens D5000), field emission scanning electron microscopy (FESEM, Tescan, Mira 3 Czech Republic) and transmission electron microscopy (TEM, Phillips 208m) were utilized. Energy-dispersive X-ray spectroscopy (EDS, DXPeX10 P Digital X-Ray Processor) was used to analyze the elements.

2.4. Mechanical characterization

Vickers microhardness (HV) of the specimens was examined using the Digital Micro Hardness Tester (HUAYI HVS-1000A, Shanghai Bimu Instrument Co., Ltd., China) at a peak load of 1 N for a duration of 15 s. Each sample was examined in six various locations and six specimens were examined for each group. Compressive tests at room temperature on a universal tensile machine were utilised to analyze the mechanical characteristics of the composites. Cylindrical specimens were machined along the extruded direction. A compressive test was performed with a constant cross-head speed and a strain rate of 10^{-4} s. To ensure repeatability, at least three samples of each mixture were evaluated.

2.5. Immersion and electrochemical tests

The electrochemical corrosion experiments of the specimens were done in the simulated body fluid (SBF) medium at 37°C. The cold mounted specimens were utilized as working electrode in a three-electrode system arrangement with a platinum electrode (10 cm^2) as the counter electrode, and a saturated calomel electrode (SCE) as the reference electrode. The potentiodynamic polarisation plots were obtained utilizing a multichannel potentiostat (VSP-300 multi), which recorded the potential every 10 mV between 1 and 2 V. The corrosion rate (mm/a) and corrosion current density (i_{corr}) were determined using the Tafel extrapolation technique. After achieving a stable open circuit potential (OCP), the AC voltage impedance analyzer was used to investigate electrochemical impedance spectroscopy (EIS) (solartron, 1260). The frequency was altered between 10^{-1} and 10^5 Hz. The program (ZsimpWin Version 3.4) has been utilised to evaluate EIS data and find an optimum equivalent circuit model. The corrosion properties of the samples were studied under physiological pH conditions with a Kokubo solution. The corrosion rate was determined by collecting the hydrogen produced by the reaction of Mg with SBF solution. Cylindrical samples were pasted at the bottom of a 1000 mL beaker containing 800 mL SBF solution. All specimens were mounted in epoxy resin with an exposed area to the corrosive environment of 0.785 cm^2. Eventually, the samples were weighed, then they were immersed for 168 h in the SBF at 37°C to perform weight loss experiments. To eliminate the corrosion products, the samples were cleaned in a boiling solution containing 15wt% CrO_3 + 1wt% $AgCrO_4$ in 100 mL of water for 1 min before being rinsed with acetone. Then, the weight loss for every specimen was calculated and utilized to determine the corrosion rate. Then every experiment was performed 3 times to guarantee repeatable findings. A test sample that was submerged in the same solution and maintained at the same temperature was utilized to assess pH changes during the study. A pH meter (PHS-3C, China) has been used to determine the pH. Scanning electron microscopy (SEM) was employed to study the surface characteristics and energy dispersive X-ray spectroscopy (EDS) was used for the elemental analysis. After each immersion time, the concentration of Mg^{2+} ion release in the SBF was also measured by atomic absorption spectroscopy (AAS, SHIMADZU, Japan).

2.6. Cell culture tests

According to the ISO 10993-5 standard, MG63 human osteosarcoma cell line was used to study the specimens' cell toxicity. The cells were cultured in Dulbecco's modified Eagle's medium (DMEM) with 10vol% fetal bovine serum (FBS), 100 g/mL streptomycin, and 100 U/mL penicillin in a

humidified environment of 5vol% CO_2 at 37°C. The surface area of the samples to extraction volume ratio was 1 cm^2/mL. 3-(4,5-dimethylthiazol-2-yl)-2,5-diphenyl-2H-tetrazolium bromide (MTT) assay results are more fully described according to [45]. The MG63 cells were seeded on culture plates under test-like circumstances as a control. Alkaline phosphatase (ALP) performance was evaluated to investigate the differentiation activity of MG63 cells after 3 and 7 d of culture. The cells were washed three times with phosphate buffered saline (PBS) that had a pH value of 7.4 until being trypsin-EDTA detached [48].

2.7. Statistical analysis

The results of independent studies were evaluated utilizing SPSS 19.0 software and presented as mean ± standard deviations. And Student's t-tests were carried out between different groups to calculate the values of p, which were significant when $*p < 0.05$.

3. Results and discussion

3.1. Microstructure

Fig. 2 presents the morphology of the refined Mg alloy, GNS, MgO@GNS, GNS/Mg, and MgO@GNS/Mg nanocomposite powders. The Mg powder is reduced in size during refinement (milling), taking on a flaky form with a diameter of 50 to 20 µm (Fig. 2(a)–(c)). The friction and impact during the ball milling process cause the form and dimension changes, flattening the powder [1]. It is worth noting that the specific surface area of these flaky powders is similar to that of 2 µm width. The refinement procedure significantly enhanced the surface area of the Mg powder and provided a homogeneous mixing of Mg and GNS composite powders. As presented in Fig. 2(d)–(f), the thin, wrinkled texture and large surface area of the GNS contributed to the formation of the wrapping effect. In this research, the statistically average width and length of the GNS were 1 µm and 2.20 µm, respectively (Fig. 2(f)). It was possible to see the sheet-like structure of GNS with the covering of vast surface wrinkles, which is a common characteristic of GNS [49].

The GNS was observed to be dispersed uniformly among the Mg alloy particles in the mixed MgO@GNS/Mg powder (Fig. 2(g)). TEM micrographs of the MgO@GNS nanohybrid revealed that MgO was evenly dispersed and adhered to the GNS surface (Fig. 2(h)). The magnified image reveals that GNS wrapped the Mg alloy particles so close (Fig. 2(i)). The complete wrapping underlined strong protection and desirable affinity of GNS to Mg alloys. These findings indicated that GNS could be evenly dispersed in mixed powders and tightly wrapped Mg alloy particles [50]. The morphology of the composite powder is shown in Fig. 2(g). Semi-powder metallurgy was used to embed the MgO@GNS nano reinforcement evenly in the Mg alloy. The refinement procedure of Mg powder, which not only lowered particle size but also altered particle shape from spherical to flaky, aided the mixing process, allowing MgO@GNS to be more evenly incorporated in the Mg alloy powders.

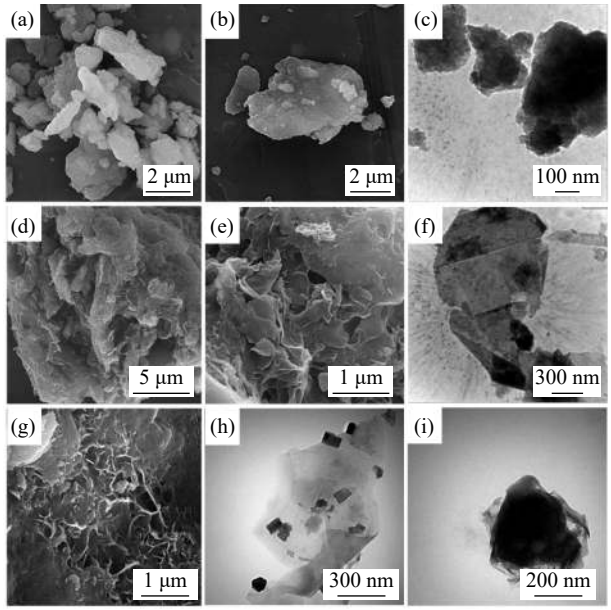

Fig. 2. (a, b) SEM images of Mg alloy powders, (c) TEM image of Mg alloy powders; (d, e) FE-SEM micrographs and (f) TEM analysis of graphene nanosheet (GNS) powder; (g) SEM image of MgO@GNS/Mg nanocomposite powders; (h) TEM image of MgO@GNS powder; (i) TEM image of wrapping Mg alloy powder by GNS.

Fig. 3(a) shows sufficient dispersion of MgO@GNS nanohybrid that should operate as a stronger reinforcement material for the Mg matrix, resulting in synergistic effects. The GNS tends to agglomerate, although the existence of MgO particles on the surface of GNS results in strong interfacial bonding between Mg and GNS and prevents self-agglomeration and clustering tendency because of the large surface area [20,51]. The carboxylic acid functional groups on GNS make them negatively charged in an aqueous solution, inhibiting re-aggregation because of strong Van der Waals interaction. Furthermore, the attractive π–π interactions among GNS predominate against the electrostatic repulsive forces due to the presence of MgO on GNS, leading to the creation of an interconnected network [52]. Raman spectroscopy was used to investigate the structural characteristics of GNS after functionalization, as shown in Fig. 3(b). Two significant peaks for GNS were observed at 1586 and 1335 cm^{-1} that match well-recorded G and D bands, respectively. The intensity of D-band to G-band (I_D/I_G) was also used to give details about defects of structure in the MgO@GNS/Mg composite [53]. Moreover, graphene nanosheets show a significant peak at 2700 cm^{-1} that is assigned to 2D band created by oxidation defects [33]. Similarly, it was reported that the integrated I_D/I_G is a ratio that indicates the degree of defects present in graphene nanosheets. A higher ratio indicates more defects. As shown, after the incorporation of MgO on GNS (MgO@GNS) and loaded with Mg alloys matrix (MgO@GNS/Mg), ID/I_G is around 1.33, which is higher than that of raw GNS (0.55), revealing that structural defects of GNS were manufactured in the semi powder metallurgy method and the formation of non-sp^2 defects in GNS occurred during the dispersion process [53–55].

Furthermore, the XRD analysis (Fig. 3(c) and (d)) validated the Raman results. Fig. 3(c) shows the XRD patterns of GNS. There was diffraction peaks in the vicinity of 2θ at about 26.5° and 43°, as shown in Fig. 3(c). The GNS has a strong (002) peak and a very low intensity peak near (100) peak [53]. In the XRD pattern, the diffraction peaks of Mg and MgO were identified in the MgO@GNS/Mg composite, while the GNS diffraction peak was not found. It's probable that the content of GNS was low so not to be detected by the XRD instrument or that GNS was well exfoliated and distributed in the matrix, where regular and periodical GNS arrangement was eliminated [53]. The peaks at 2θ equal to 32°, 34°, and 36° represent prism $\{10\bar{1}0\}$, basal {0002}, and pyramidal $\{10\bar{1}1\}$ planes of HCP crystal structure of Mg (Fig. 3(d)). It can be noticed that basal plane intensity increases with addition of MgO@GNS. It means that the addition of MgO@GNS into alloy matrix has changed the orientation of Mg orientation or crystallographic texture. Atomic force microscopy (AFM) was used to examine the composite surface roughness. Fig. 3(e) presents AFM morphology and surface roughness of Mg alloy matrix, GNS/Mg and MgO@GNS/Mg nanocomposites. The surface of the GNS/Mg composite has features similar to length of sand dune structure with gullies and many valleys, as illustrated in Fig. 3(e). The surface roughness (R_a) of the GNS/Mg nanocomposite was 287 nm, while with the addition of MgO@GNS nanohybrids, the surfaces of MgO@GNS/Mg become wrinkled and lower peaks are detected on the surface (R_a = 226 nm), indicating MgO@GNS nanohybrids have tightly incorporated in Mg-based composite surface [56]. The hydrophilic property of the Mg matrix, GNS/Mg and MgO@GNS/Mg nanocomposites was evaluated using hydrophilicity analysis, and the results are given in Fig. 3(f). High contact angle (CA) values represent hydrophobicity, whereas low angles represent hydrophilicity. The Mg alloy was relatively hydrophobic (78°). Incorporation of GNS in the Mg matrix boosted surface wetting to 68° due to the hydrophilic nature of GNS. However, MgO@GNS incorporation significantly decreased water CAs to 53° due to the presence of MgO particles, which decreased composite surface roughness [57].

The intensity variations of the pyramidal, basal, and prismatic planes can be influenced by the presence of additive phase in the Mg matrix [58]. As a result, Fig. 4(a) and (b) shows {0002} pole figures obtained from the Mg matrix and produced composite, as well as variations in the intensity ratio of basal planes multiples of random distribution. Changes of the basal planes multiples intensity ratio of random distribution ($I(0002)/I(10\bar{1}1)$) for Mg alloy and MgO@GNS/Mg are 0.42 and 1.13, respectively. According to XRD patterns in Fig. 3(d), incorporating nanohybrid reinforcement has increased the basal texture intensity. The pole figures in Fig. 4(a) and (b) depict the fiber texture, which results from the arrangement of normal basal planes in radial directions as a result of grain rotation. The appropriate distribution of

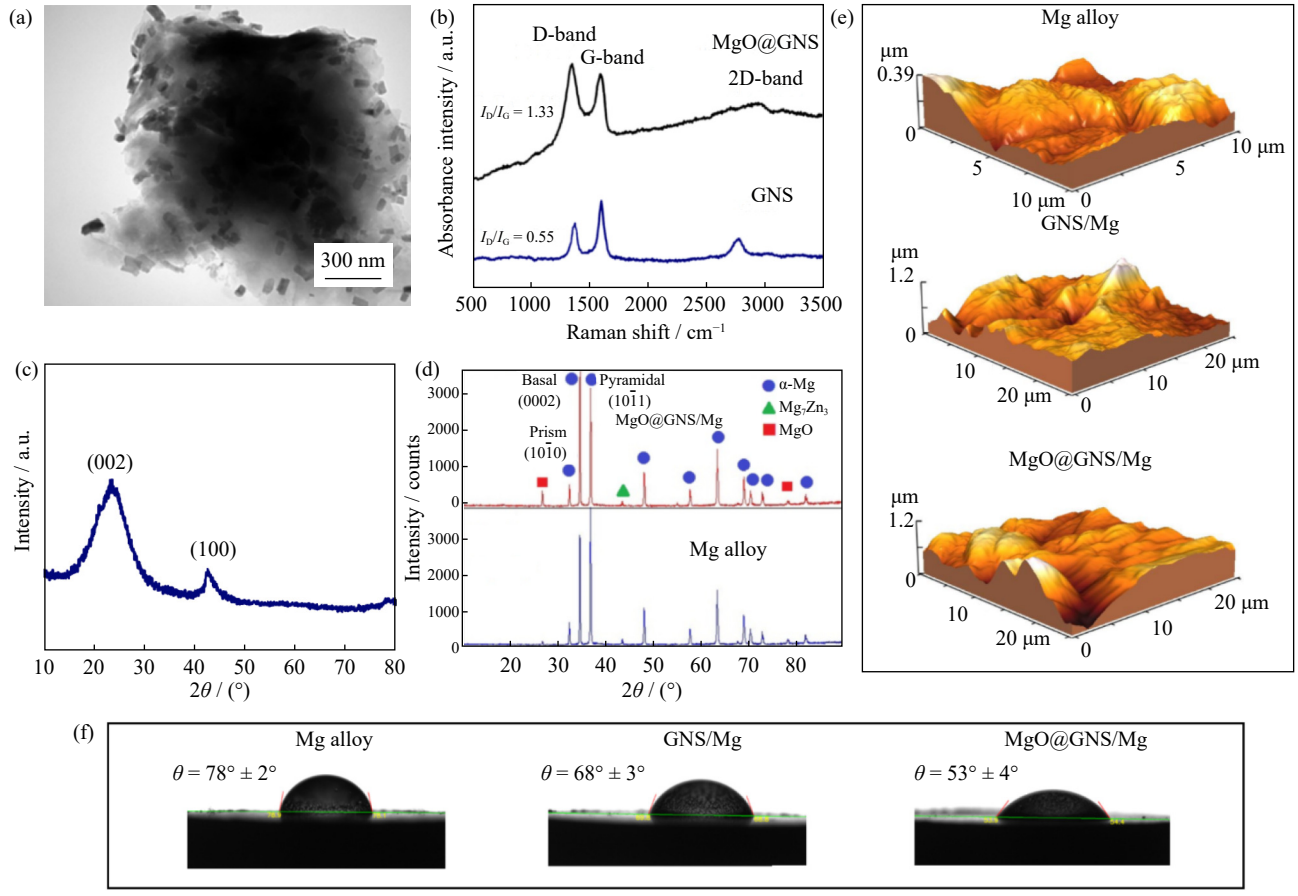

Fig. 3. (a) TEM micrograph of MgO@GNS power; (b) Raman spectra of GNS and MgO@GNS powders; XRD patterns of (c) GNS and (d) Mg alloy and MgO@GNS/Mg nanocomposite; (e) AFM images; (f) water contact angles (WCAs) images of specimens.

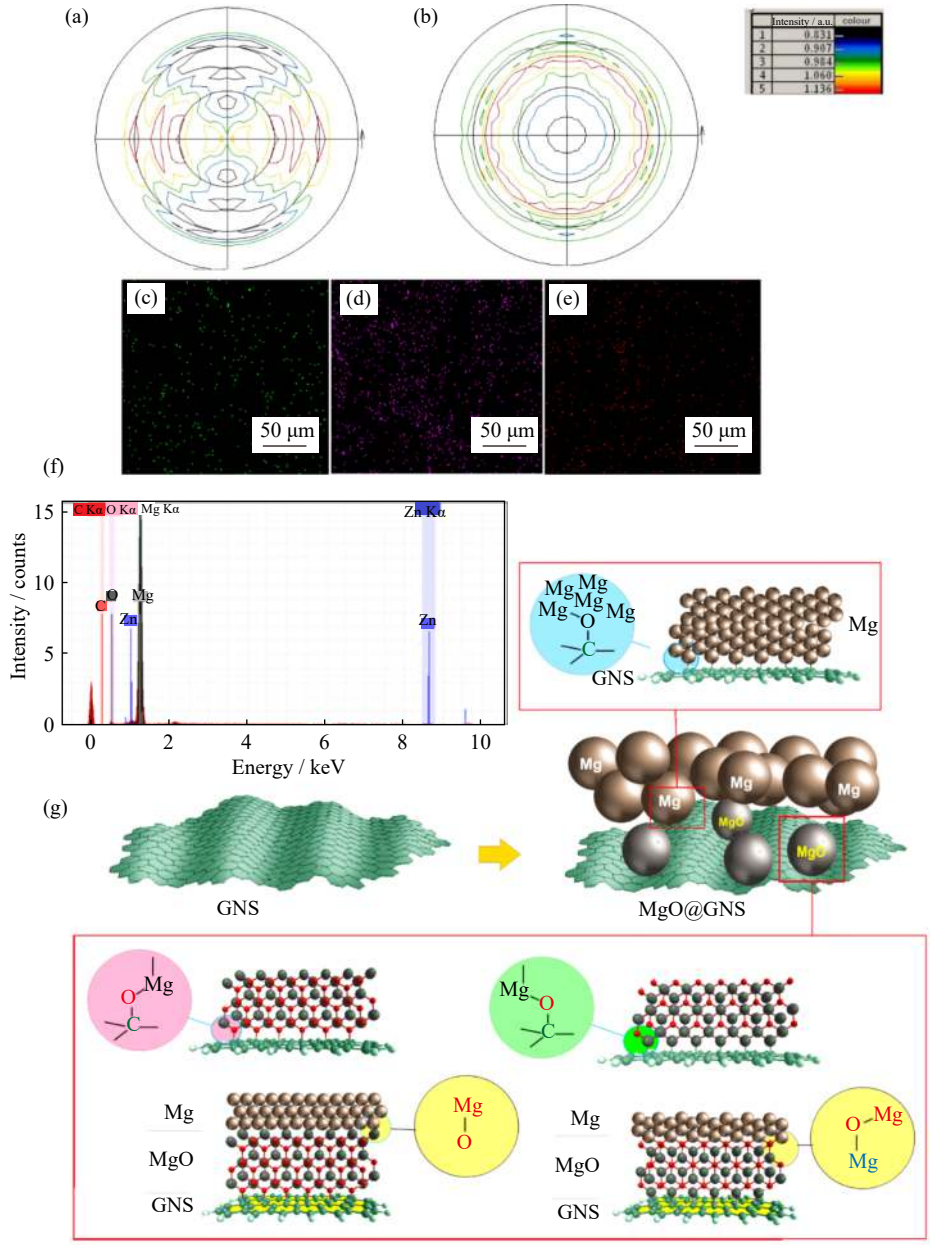

Fig. 4. Pole figures for {0001} obtained from the (a) Mg alloy and (b) MgO@GNS/Mg composite; elemental mappings of the MgO@GNS/Mg composite: (c) O, (d) C, and (e) Zn element; (f) EDS spectrum corresponding to nanocomposite; (g) schematic illustration the interface of Mg/GNS, Mg/MgO, and GNS/MgO.

MgO@GNS in Mg alloy during the fabrication process leads to grain rotation and increases the intensity of the texture, which may cause the texture randomization [59]. Related EDX elemental maps of MgO@GNSMg sintered sample and corresponding EDS analysis of nanocomposite are shown in Fig. 4(c)–(f), illustrating the distribution of Zn, GNS, and MgO in the Mg matrix. It was revealed the Zn, C and O had even distribution in the Mg alloy. The uniform dispersion of particles influences the corrosion and mechanical characteristics of Mg matrix composite. The oxygen and carbon distributions representing GNS and MgO were uniform, showing the effect of the semi powder metallurgy technique on MgO@GNS nanohybrid distribution in the Mg alloy matrix [60]. The uniform dispersion of GNS was difficult and could construct an agglomeration structure and several inner imperfections in the metal matrix [44]. GNS are covered by the MgO nanoparticles in this study resulting in a lower their tendency to agglomerate, allowing them to disperse uniformly in the Mg matrix [61].

The schematic illustration of GNS–MgO–Mg interface is established in Fig. 4(g). The MgO nanoparticles attached to GNS and Mg provide an effective driving force for Mg to wet and spread on the surface of GNS [62]. The semi coherent interface generally has a relatively low interfacial energy, which assists in the establishment of solid interfacial bonding between MgO and Mg metal matrix. Also, the presence of MgO nano reinforcements at the interface can facilitate a tight connection between the GNS and Mg matrix, effectively increasing interfacial interaction bonding strength and load transfer mechanism efficiency [49,61]. Therefore, the

MgO nanoparticles covering GNS can enhance the graphene dispersion and the *in situ* reaction between the MgO and Mg matrix, improving interfacial wettability.

3.2. Mechanical characteristics assessment

Table 1 and Fig. 5(a) represent the Vickers hardness test results. The hardness values for Mg alloy and GNS/Mg composites are HV 59.1 ± 5.7 and 84.3 ± 7.2, respectively. The hardness value of composite (GNS/Mg) is 42.5% higher compared to Mg alloy. The hardness enhanced more with the addition of MgO, wherein the hardness value for MgO@GNS/Mg nanohybrid composites was HV 91.2 ± 6.5 (54.2%). In this regard, the existence of GNS and MgO nanoparticles in the composite acts as a barrier which leads to grain refinement and enhancement of the hardness. The decrease in Mg particle size has a favorable influence on the hardness values. Furthermore, the appropriate dispersion of nano-MgO attached GNS reinforcement in the Mg-matrix improves overall hardness since this nanohybrid reinforcement (MgO@GNS) is hard to deform and impedes dislocation motion [63]. It has been observed that during extrusion, the limitation on the reinforcement layers imposed via the Mg flakes causes MgO@GNS nanohybrid filler layers to move mostly in planar orientations, causing them to arrange along the extrusion orientation. Therefore, the nanohybrid filler (MgO@GNS) was properly aligned after extrusion, which increased the composite hardness in addition to maintaining the lamellar structure [52].

Table 1. Mechanical properties of samples

Sample	UCS / MPa	Failure strain / %	Microhardness, HV
Mg alloy	288.3 ± 12.4	8.3 ± 1.3	59.1 ± 5.7
GNS/Mg	324.5 ± 13.1	9.7 ± 1.5	84.3 ± 7.2
MgO@GNS/Mg	358.6 ± 13.7	10.5 ± 1.3	91.2 ± 6.5

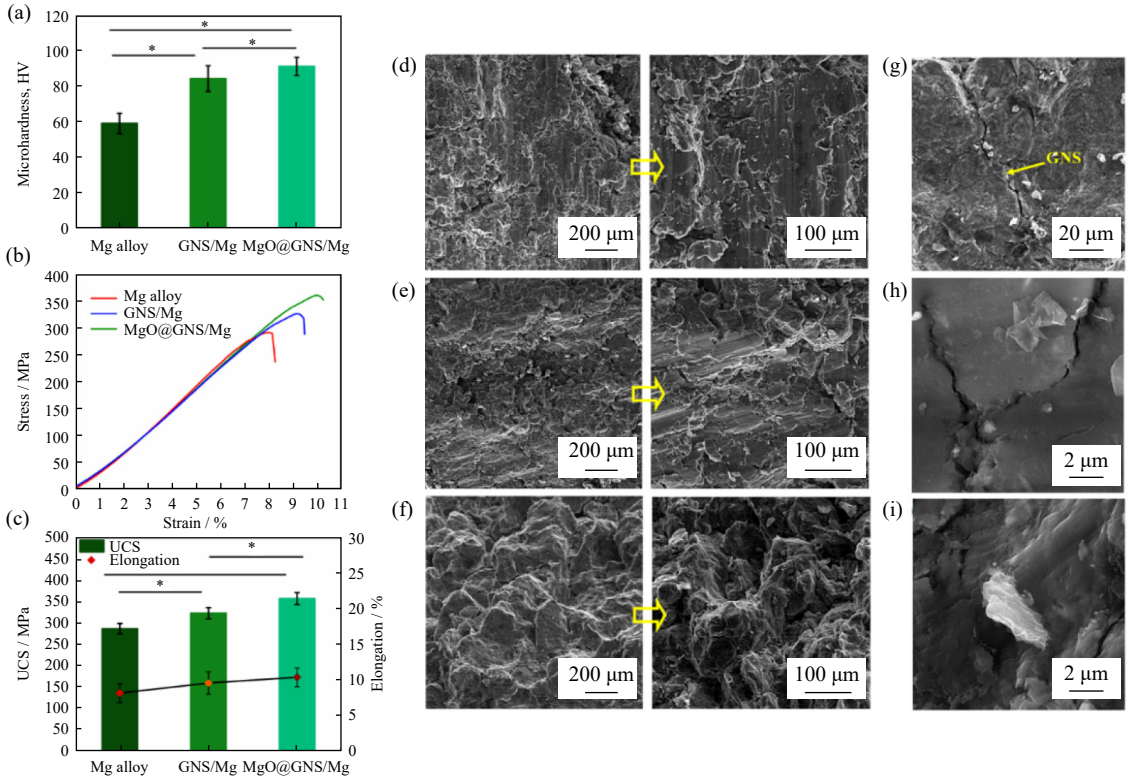

Fig. 5. (a) Microhardness values, (b) compressive stress–strain curves of the matrix and nanocomposites, and (c) changes of ultimate compressive strength (UCS) and failure strain of Mg matrix, GNS/Mg composite, and MgO@GNS/Mg composite (*p < 0.05). SEM micrographs of fracture surfaces of (d) Mg alloy, (e) GNS/Mg composite, (f) MgO@GNS/Mg composite. SEM images of (g) crack along grain boundary in fracture surface, (h) crack branching, and (i) GNS pull out mechanisms of MgO@GNS/Mg composites.

Fig. 5(b) and (c) shows the compression test results of Mg alloy, GNS/Mg, and MgO@GNS/Mg nanocomposites at room temperature. These findings show that the compressive properties of the GNS/Mg nanocomposite, such as failure strain (9.7%) and ultimate compressive strength (UCS, 324.5 MPa) enhanced when MgO@GNS was added to the Mg matrix composite (failure strain: 10.5% and UCS: 358.6 MPa). Nevertheless, the Mg alloy showed compressive strength (UCS) of 288.3 MPa and failure strain of 8.3% (Table 1). The addition of MgO@GNS nanohybrid reinforcement greatly improved the compressive strength according to the compressive and hardness experiments. It is

also important to consider the particle reinforcing effect of the uniformly distributed MgO@GNS nanohybrid fillers in the Mg alloy matrix [35,64]. The homogeneously distributed MgO@rGO hybrid fillers with higher hardness could act as a strengthening agent by the means of load transfer and crack deflection, enhancing the resistance of the Mg alloy matrix to external forces. As an external force was applied to the matrix, the solid MgO@GNS nanohybrid reinforcements may provide a stress concentration effect that could readily cause microcracks in the surrounding matrix and absorb specific energy of deformation [65]. The plastic deformation was developed by the interface between the MgO@GNS nanohybrid filler and the Mg matrix. Furthermore, the MgO@GNS hybrid inhibited crack propagation, preventing it from developing into breaking.

The compressive fracture surfaces of Mg alloy, GNS/Mg and MgO@GNS/Mg composites often exhibit shear bands with no apparent voids (Fig. 5(d)–(f)). Finally, the fracture surface property is consistent with the mechanical characteristics of the related composites. Overall, well-dispersed GNS can contribute to improved mechanical properties through effective load transfer, whereas GNS clusters weaken the strengthening effect and even mechanical characteristics, owing to poor bonding between layers of graphene [66]. The existence of MgO nanofillers on the high specific surface area of graphene nanosheets might inhibit GNS aggregation because of their strong interlayer π–π stacking interaction [41]. In fact, MgO nanoparticles and GNS functioned together to increase the interparticle space of MgO nanoparticles and the interlayer space of GNS, which inhibited aggregation and promoted dispersion [10]. More importantly, semi powder metallurgy and hot extrusion enables high strengthening efficiency and proper mechanical characteristics of GNS/Mg nanocomposites by tailoring factors such as the distribution of GNS and MgO@GNS fillers, secondary phase as well as microstructural defects [67]. The results demonstrate that the fracture surface of the MgO@GNS reinforcement-encapsulated Mg matrix composite has no obvious dimples or cleavage platforms (Fig. 5(f)). A common crack seen from the fracture surface of MgO@GNS/Mg specimen is shown in Fig. 5(g). It is seen that the crack is mainly along grain boundary, indicating that the fracture was initiated from microcracks formed along grain boundaries. Fig. 5(h) illustrates the crack branching mechanism by GNS in nanocomposites and Fig. 5(i) demonstrates considerable pull-out of GNS on the fracture surface of MgO@GNS/Mg sample. This indicates that the effects of MgO@GNS on bridging and obstruction of dislocation are helpful for load transfer and increasing the bearing capacity of the matrix, which was essential for strengthening and ductility to a certain extent [10,66]. Understanding strengthening mechanisms is crucial. The role of nanohybrid filler type in microstructural assessment must be studied for a reliable characterization of mechanical properties. The following reasons contribute to the increased compressive strength, failure strain, and microhardness of MgO@GNS/Mg composites: (i) dislocation multiplication because of a mismatch in the coefficient of thermal expansion (CTE) between reinforcement (MgO@CNTs) and Mg alloy, (ii) Orowan mechanism, (iii) grain refinement, and (iv) the efficient load transfer from the Mg matrix to the additive due to the strength of improved interfacial bonding with MgO nanofillers [68]. Furthermore, in MgO@GNS/Mg composites, the dominant strengthening mechanism is load transfer which may also considerably increase the usage efficiency of the inherent features of nanohybrid reinforcement [49]. Load transfers from the soft Mg matrix phase to the hard reinforcement due to load transfer mechanism when the material is subjected to external loading. The applied stress is held at a high level corresponding to load bearing due to the great plastic strain field caused by the high accumulation or tangle of dislocations near the GNS [69–70]. The incorporation of MgO@GNS into the Mg-based composite improved yield strength via the load-transfer mechanism [71].

3.3. *In vitro* biocompatibility

Osteoblast cell attachment to the implant surface is necessary for their growth and the creation of mineral deposits. Moreover, it is vital in osseointegration which specifies the lifetime of the implants. Fig. 6(a)–(c) shows that the number of adherent MG63 cells osteoblasts increases after addition of GNS and MgO@GNS into the Mg matrix after 7 d. It is clear that the GNS/Mg and MgO@GNS/Mg nanocomposites have more MG63 cells adhering to their surfaces than the Mg alloy. The osteoblasts on the surface of each sample are elongated and flat with a good spread, firmly showing that the addition of MgO@GNS has a minimal favorable influence on the osteoblast spreading on the Mg alloys resulting in its great biocompatibility [72]. Furthermore, the nanoscale topography of the surface of the GNS/Mg and MgO@GNS/Mg composites influences osteoblast activities such as proliferation and adhesion with wide nanosheets (>100 nm) are favorable particularly for adhesion of osteoblasts. Because serum contains fibronectin that aids in cell adhesion, there is a close relationship between subsequent cell growth and the adsorption ability of the substrate for serum proteins. It has been found that GNS has a greater ability for serum protein adsorption. As a result of the presence of GNS, great adhesion molecule supply promotes cell attachment and proliferation. As a result, both MgO and GNS co-contribute to the early spread and proliferation of cells [34].

The hydrophilic surface of the samples improves osteoblast attachment, osseointegration, bone mineralization, and differentiation [48]. Shi *et al.* [73] found that the addition of GO in the composite coating promotes cell proliferation and improves bone cell adhesion and proliferation on 2GO/HA coated samples.

The MTT assay findings in Fig. 6(d) similarly demonstrate an improvement in cell viability when osteoblast cells are cultured with MgO@GNS/Mg and GNS/Mg composites. According to the findings, it is possible to deduce that modifying the topography of the surface by the addition of MgO@GNS in Mg matrix composite and the existence of graphene sheets may be beneficial for the proliferation and adhesion of cells. This is because certain biomolecules, like

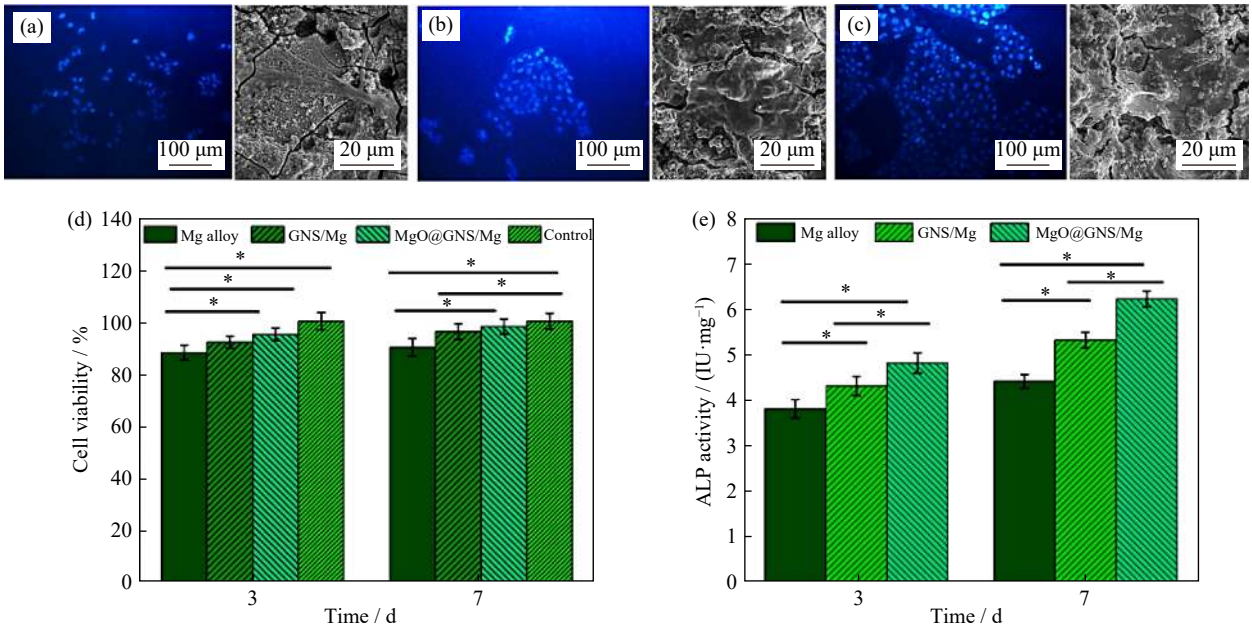

Fig. 6. Fluorescent microscopic and SEM images of MG63 cells on (a) Mg matrix, (b) GNS/Mg, and (c) MgO@GNS/Mg composites after 7 d; (d) MG63 cell viability and (e) ALP activity on Mg alloy matrix, GNS/Mg and MgO@GNS/Mg nanocomposites after 3 and 7 d (*p < 0.05).

proteins, preferentially adsorb on nanostructure materials with nano-rough surfaces and functional groups on the GNS [74]. Remarkably, the cell attachments to the biomaterial are caused by the interaction of its integrins with these adsorbed proteins [48]. Furthermore, the incorporation of MgO nanoparticles substantially increased the cell viability and proliferation on the surface of the specimens. Therefore, it can be hypothesized that the Mg^{2+} ion released from the surface of the implant aided in the ability of MG-63 cells to adhesion and multiplication [75].

To investigate the osteoinductive capacity of the Mg alloy matrix and the GNS/Mg and MgO@GNS/Mg nanocomposites, ALP activity as one of the early osteogenic differentiation markers was evaluated after 3 and 7 d. The ALP activity of MG63 cells cultured on MgO@GNS/Mg samples was greater than those of GNS/Mg composite and Mg alloy. As shown in Fig. 6(e), MgO@GNS nanohybrid reinforcements had a beneficial effect on MG63 osteogenic differentiation. It is important to note that the good cell response can be related to a lower corrosion rate and therefore reduced pH increase and ion release, both of which were considered to possess a considerable effect on cell growth [42,48]. GNS can enhance the adhesion, proliferation, and osteogenic differentiation of mesenchymal stem cells because of its high biocompatibility [34,76].

3.4. Corrosion and immersion tests

Potentiodynamic polarization tests were done in SBF for the matrix and nanocomposites to analyze the corrosion protection characteristics afforded by the MgO@GNS filler. Fig. 7(a) shows the typical polarization plots. Corrosion current density (i_{corr}) and corrosion potential (E_{corr}) were directly determined by the potentiodynamic polarization plots using the Tafel region extrapolation method. Table 2 displays the relevant Tafel data. E_{corr} of MgO@GNS/Mg and GNS/Mg composites were −1.19 and −1.31 V after the filler was added, respectively.

The i_{corr} values experienced a considerable decrease from 127.7 to 99.1 μA/cm^2 related to Mg alloy and GNS/Mg composite, respectively. The incorporation of GNS into the composite considerably decreases the corrosion rate of Mg alloy matrix. The i_{corr} values decreased dramatically from 99.1 μA/cm^2 for GNS/Mg to 80.4 μA/cm^2 for MgO@GNS/Mg composite. Furthermore, the corrosion rate (C_R) values for Mg alloy decreases from 2.92 to 2.26 and 1.84 mm/a with the addition of GNS and MgO@GNS fillers, respectively. As it is well known, the porosity and chemical composition of the composites affect their corrosion resistance [77]. Therefore, with the addition of MgO@GNS fillers, the i_{corr} and corrosion rate decrease because the presence of GNS and MgO nanoparticles in the composites decreased the opening defects, micro-cracks, and micro-pores of the composites and as a result, aggressive Cl^- ions penetrate to the substrate. It may be seen as a result of micro-pores filling with MgO@GNS fillers, which slows the entry of corrosive ions. The decreased corrosion rate in the composite implies that these nanosheets could operate as a good barrier because of the high chemical stability of GNS in SBF [33,78]. Shuai *et al.* [42] have successfully synthesized AZ61 alloys reinforced with RGO/MgO via selective laser melting (SLM) to strengthen the interfacial bonding between Mg matrix and RGO. Abazari *et al.* [48] have fabricated ZM31/*x*RGO biocomposites by semi-powder metallurgy technique. The results show that the corrosion current density of AZ61-3.0RGO/MgO was 42 μA·cm^{-2}. The corrosion current density of ZM31-0.5RGO and MgO@GNS/Mg were 96.4 and 80.4 μA·cm^{-2}, respectively. Therefore, it was concluded that the SLM process was better method than SPM due to

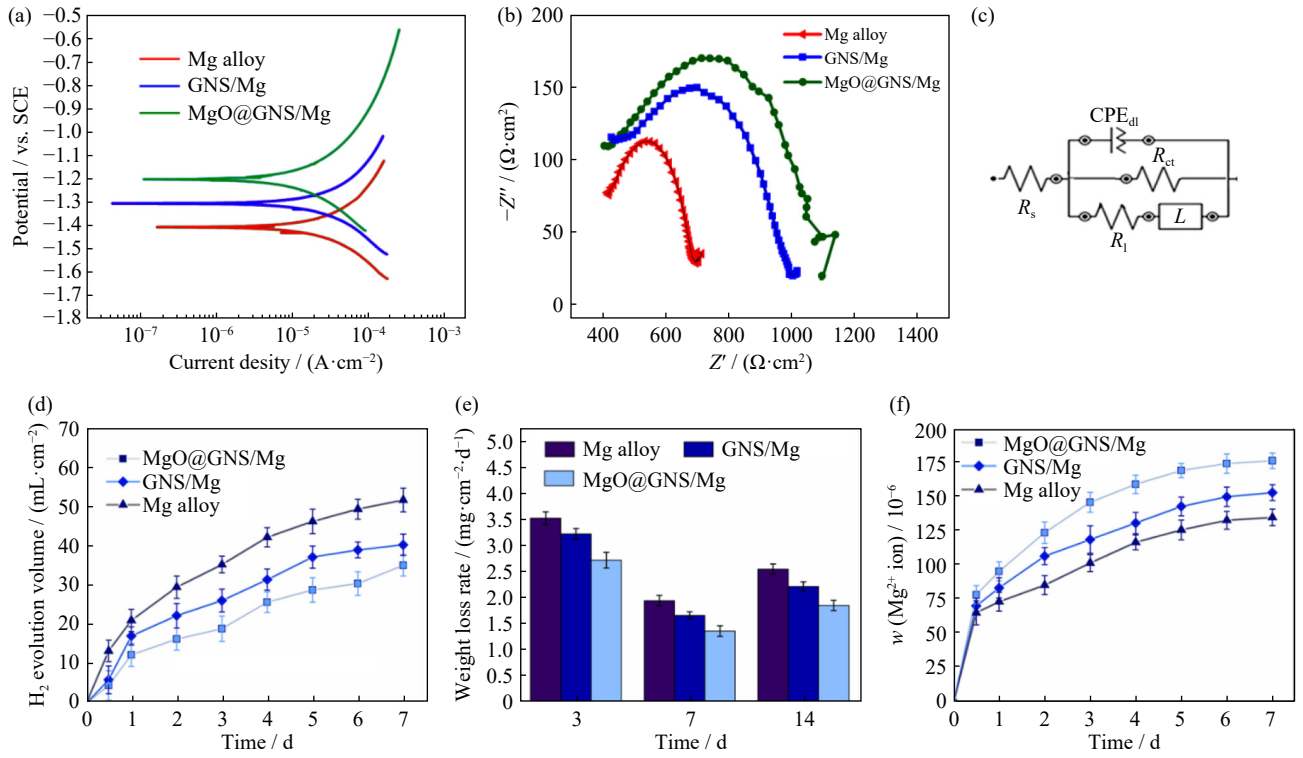

Fig. 7. (a) Polarization curves; (b) Nyquist curves; (c) equivalent circuit model for samples in SBF (where CPE_{dl} and R_{ct} are the double-layer capacitance and the charge transfer resistance, respectively, R_s is the electrolyte resistance, R_l shows a high-medium frequency capacitive loop, and L has named as the inductive function); (d) H_2 gas evolution volume, (e) weight loss rate, and (f) Mg^{2+} ion release content of Mg alloy, GNS/Mg composite, and MgO@GNS/Mg composite after immersion for 7 d in SBF solution.

Table 2. Electrochemical data acquired from polarization and Nyquist curves

Sample	E_{corr} / V vs. SCE	i_{corr} / (μA·cm^{-2})	C_R / (mm·a^{-1})	R_{ct} / (Ω·cm^2)
Mg alloy	−1.41 ± 0.014	127.7 ± 11	2.92 ± 0.32	163.4 ± 17.96
GNS/Mg	−1.31 ± 0.021	99.1 ± 8	2.26 ± 0.26	277.2 ± 21.51
MgO@GNS/Mg	−1.19 ± 0.018	80.4 ± 10	1.84 ± 0.29	314.5 ± 27.68

strengthening the interfacial bonding of Mg-based composite with MgO as interfacial bridges and further the bulk characteristics.

Fig. 7(b) shows the Nyquist plots for the Mg matrix and GNS/Mg and MgO@GNS/Mg nanocomposites in the SBF solution. The charge transfer resistance (R_{ct}) could determine the corrosion protection of the composite system, which is inversely related to the corrosion rate [69]. According to the Nyquist impedance diagrams, the GNS/Mg and MgO@GNS/Mg composites have similar properties as the Mg alloy. The only difference is that the R_{ct} of the GNS/Mg and MgO@GNS/Mg composites is evidently higher than that of the Mg alloy (Fig. 7(b)). The equivalent circuit was employed to fit the obtained Nyquist impedance spectra as shown in Fig. 7(c). Also immersion tests were employed to explore the long term degradation performance of these samples using hydrogen (H_2) gas evolution and weight loss tests to further expose the corrosion behavior of these composites (Fig. 7(d) and (e)).

During the hydrogen gas evolution test, numerous bubbles were detected boosting from the Mg based surface, but few bubbles were found on the surface of the MgO@GNS/Mg sample. Furthermore, the total H_2 gas evolution content of MgO@GNS/Mg composite alloy was 34.9 mL·cm^{-2} at 168 h, which was less than Mg alloy (51.4 mL·cm^{-2}), showing a decreased corrosion rate. Moreover, weight loss tests were also used to determine the corrosion rates of Mg alloys and composites. The corrosion rates of Mg matrix, GNS/Mg, and MgO@GNS/Mg samples measured using *in vitro* immersion test differed in the range of 2.92, 2.26, and 1.84 mm/a, respectively. The total deterioration duration must be greater than 20 months as determined by an *in vivo* animal model. Even though the bone regeneration duration varies depending on clinical situations, mechanical integrity should just be preserved for 3–6 months. These findings indicate that the degradation periods of present MgO@GNS/Mg composites correspond to the period of bone regeneration in the human body. In other words, the appropriate corrosion behavior of the MgO@GNS/Mg composite can lead to an outstanding match between the bone healing time and the degradation duration [75]. In this regard, Shuai *et al.* [50] revealed that after incorporation of GO fillers into the AZ61 alloy, GO eventually wrapped α-Mg grains and obstructed the interaction between the matrix and body fluid to some degree, thus reducing the influence of galvanic corrosion and decreasing the degradation rates. Likewise, it was reported that GO in

the corrosion layer prohibited it from falling off the Mg matrix due to the bridging influence, therefore impeding the penetration of the corrosive medium.

Fig. 7(f) presents the results of the amount of Mg^{2+} ion release content in SBF as a function of immersion time for specimens, respectively. According to the results of H_2 gas evolution, the amount of released Mg^{2+} ion was considerable during the first 24 h of evaluation. This could be due to the creation of a precipitated layer on the samples after 24 h [79]. When the samples were subjected to the SBF, chemical dissolution on the entire surface resulted in rapid degradation, which decreased gradually following corrosion product precipitation.

The surface morphologies of Mg matrix and the GNS/Mg and MgO@GNS/Mg samples are shown in Fig. 8(a) after immersion in SBF for 7 d. Mg-based alloy has been entirely corroded with a significantly rougher corrosion surface. Furthermore, corrosion cracks cover the whole sample surface. The existence of a more dense and compact construction of corrosion products on MgO@GNS/Mg composite surface can give a better level of protection in SBF than the loose corrosion product that formed on GNS/Mg composite surface and Mg alloy [80–81]. Additionally, the surface cracks on the MgO@GNS/Mg composite were smaller and shallower than those on Mg alloy, as observed in the enlarged images. After 7 d of immersion, a number of narrower mineral clusters (with a spheroidal and flat shape) were deposited on the MgO@GNS/Mg composite surface too (Fig. 8(a)). The high-magnification micrograph in Fig. 8(a) indicated that the clusters were made up of flat and spheroidal crystallites. EDS examination in Fig. 8(b) revealed phosphorus peaks in addition to calcium, magnesium, carbon, and oxygen peaks due to the presence of PO_4^{3-}, Ca^{2+}, and Na^{+} ions in the SBF solution [17,82]. As a result, the discovered needle-shape crystallites on the MgO@GNS/Mg composite can be identified as hydroxyapatite (HA) that partially protected the α-Mg matrix from the penetration of SBF, reducing the corrosion rate. It is also reported [76] that the capability of apatite formation on surfaces including GNS demonstrates that the defects of the subjected GNS in contact with SBF function as nucleation sites. The EDS spectrum in Fig. 8(b) indicated Mg and O as the primary constituents of the corrosion products of Mg alloy, implying the $Mg(OH)_2$ formation. The long-term degradation activity of biocomposites was investigated using static immersion tests. Fig. 8(c) illustrates the pH changes during Mg-based alloy, GNS/Mg and MgO@GNS/Mg samples immersion in SBF. The pH values for all samples increase significantly in the first 18 h, then increase slowly during immersion time. At the end of the immersion experiments, the pH of the immersion solution corresponding to Mg alloy, GNS/Mg composite, and MgO@GNS/Mg composite is 10.24, 10.12, and 9.78 after 168 h, respectiely. The pH values of MgO@GNS/Mg composite are always lower than those of Mg matrix, indicating that the incorporation of MgO@GNS nanohybrid reinforcement into the composite matrix decreases the degradation rate.

3.5. Antibacterial properties

Antibacterial properties of Mg matrix, GNS/Mg and MgO@GNS/Mg specimens against *S. aureus* as Gram-posit-

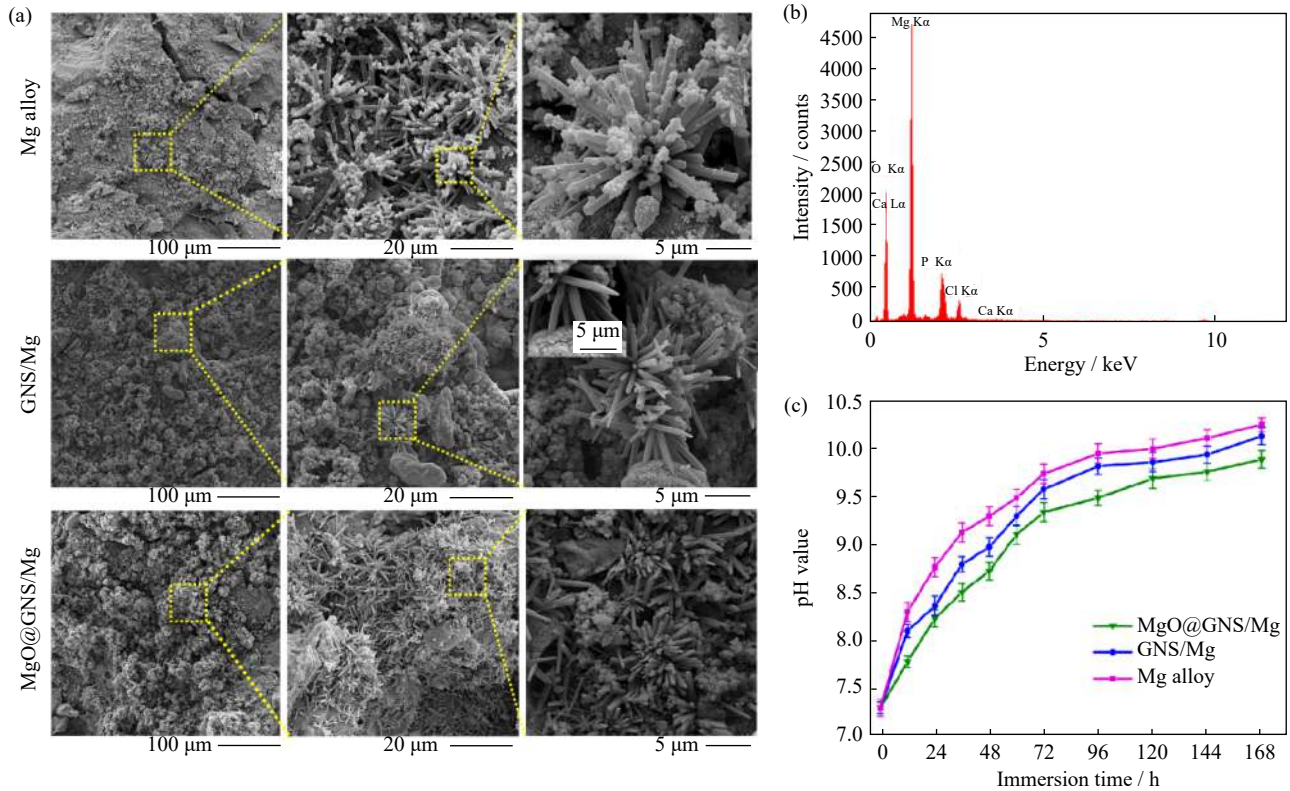

Fig. 8. (a) SEM images of Mg alloy, GNS/Mg and MgO@GNS/Mg specimens after immersion for 7 d in SBF, (b) EDS spectra of MgO@GNS/Mg sample, and (c) pH values of samples after immersion for 7 d in SBF.

ive bacteria and *E. coli* as Gram-negative bacteria were examined. The incorporation of GNS improved the antibacterial characteristics of Mg alloy considerably (Fig. 9(a)–(d)). The diameter of the inhibition zone realted to MgO@GNS/Mg composite is about (7.1±0.3) and (6.4±0.3) mm against *S. aureus* and *E. coli*, respectively, while the GNS/Mg composite has the inhibition zone diameter of around (5.5±0.2) and (4.3±0.3) mm against *S. aureus* and *E. coli,* respectively, as compared to Mg alloy with a smaller inhibition zone (Fig. 9(a)–(c)). Furthermore, the releasing of MgO was shown to boost the antibacterial activity of the MgO@GNS/Mg composite. The antibacterial test findings showed the growth in Gram-positive bacteria (*S. aureus*) is slightly higher than in Gram-negative bacteria (*E. coli*) after 24 h. The MgO@GNS/Mg composite had a much greater bacterial inhibition rate than other samples, showing that the co-incorporation of GNS and MgO fillers into the composite had a major influence on antibacterial activity [83]. It has been observed that the sharp edges of GNS could mechanically destroy the outer and inner cell membranes of bacterial cells, resulting in the release of proteins and adenine and finally, cell death [84]. Furthermore, MgO nanoparticles assist in antibacterial activity by adhering to the microbial cell membrane and penetrating the cell, creating reactive oxygen species (ROS) and causing harm to intracellular structures and biomolecules [80,85–86]. Likewise, it has been observed that both membrane and oxidative stress cause bacterial cytotoxicity. Graphene-based materials can benefit from the three-step antibacterial mechanism. In general, graphene-based compounds with a greater density of functional groups and smaller sizes have a higher probability of interacting with bacterial cells, leading to cell deposition. GNS could cause membrane stress by disrupting and destroying cell membranes, resulting in cell death by direct contact (as shown in the schematic of Fig. 9(d)) [87]. Sharp edges of graphene nanosheets may result in physical damage to bacterial membranes and release of intracellular substances, resulting in bacterial death after the attachment of GNS/Mg to bacteria [88]. This physical action mostly consists of insertion and cut, leading to high bacterial toxicity and severe cell membrane disintegration. Membrane stress in bacteria is associated with contact forms in which the lateral side with edge and corner plays a significant role than the planar surface [89]. Carbon nanotubes have also been shown to induce physical damage to bacterial membranes [90]. In other words, any graphene family nanomaterials (GFN) with a sharp edge has the potential to harm the bacterial membrane. Furthermore, membrane tension happens in a random and contact-style manner. As a result, it will be affected by material solubility and dispersity. The oxygen-containing functional groups on GO allow it to disperse more easily, giving it more opportunity to get into contact with bacteria and attain excellent bactericidal effectiveness [89–90]. Based on both analyses, the antibacterial activity of the MgO@GNS/Mg composite is related to physical damage to the bacteria membranes caused by the sharp edges of GNS and the generation of ROS by MgO nanoparticles [76]. In overall, the result is in good agreement with previous reported research [91–96] which reported that the addition of fillers such as MgO and GNS in optimum amount has a significant effect on the mechanical strength, antibacterial activity and corrosion resistance of Mg-based composites.

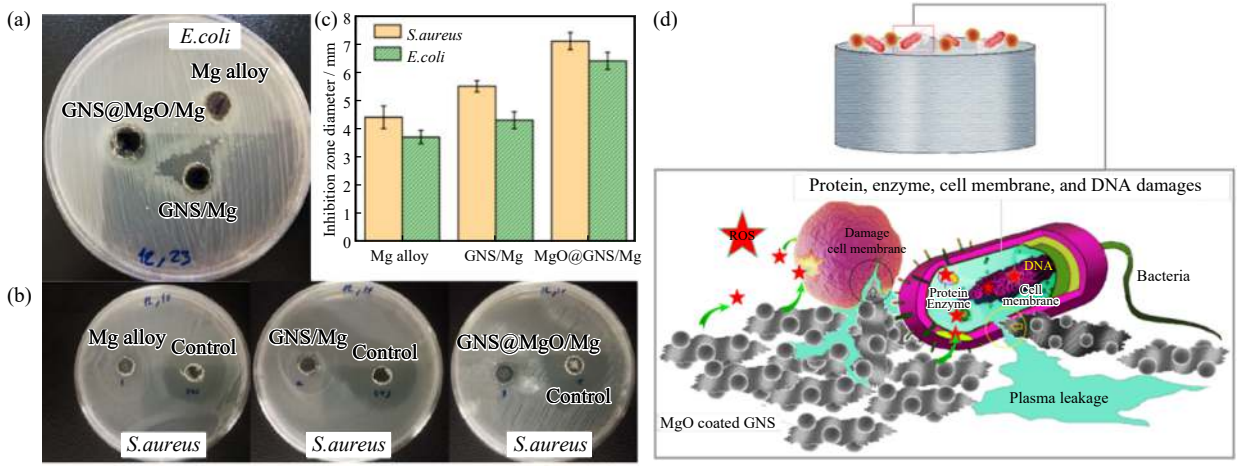

Fig. 9. Inhibition zones formed around the specimens by the disk-diffusion test against (a) Gram-negative bacteria (*E. coli*) and (b) Gram-positive bacteria (*S. aureus*); (c) the diameters of the inhibition zones; (d) schematic of the antimicrobial mechanism of MgO@GNS/Mg composite.

4. Conclusion

Mg alloy reinforced with MgO@GNS nanohybrid fillers was successfully fabricated via semi-powder metallurgy (SPM) combined with hot extrusion. Mechanical analysis revealed that MgO@GNS reinforcement increased the microhardness of Mg-based composites. A high UCS of 358 MPa and failure strain of 10.5% was achieved for the MgO@GNS/Mg composite, which could be attributed to the synergistic strengthening effect of nanohybrid MgO@rGO fillers including the optimized reinforcement distribution, high load-transfer efficiency of the MgO@rGO fillers, crack branching, and GNS pull out mechanism. The MgO@GNS/Mg composite presented the lowest corrosion rate because of the ef-

fect of the MgO@GNS nanohybrid additions, which decreased the opening defects, micro-pores, and micro-cracks of the composite and the penetration of corrosive fluid to the composite matrix. In addition to anticorrosion characteristics, the MgO@GNS nanohybrid containing Mg-based composite showed great antibacterial properties against *S. aureus* and *E. coli*, which can be greatly useful for bioimplant applications as it reduces the implant-related infection risk at the initial steps. The findings of osteoblast adhesion and apatite mineralization in SBF show that the MgO@GNS/Mg composite has better biocompatibility *in vitro* than Mg alloy. It is hypothesized that MgO@GNS hybrid additions not only provide more preferred areas for osteoblast adhesion but also create more nucleation sites, enabling apatite mineralization. This study demonstrates that the antibacterial and mechanical MgO@GNS/Mg composite could have been used in load-bearing orthopedic implants.

Conflict of Interest

The authors declare no conflict of interest.

References

[1] A. Senthil Kumar, A. Raja Durai, and T. Sornakumar, Machinability of hardened steel using alumina based ceramic cutting tools, *Int. J. Refract. Met. Hard Mater.*, 21(2003), No. 3-4, p. 109.

[2] R.B. Figueiredo and T.G. Langdon, Processing magnesium and its alloys by high-pressure torsion: An overview, *Adv. Eng. Mater.*, 21(2019), No. 1, art. No.1801039.

[3] Q.M. Dai, D.F. Zhang, J.Y. Xu, B. Jiang, and F.S. Pan, Tensile mechanical properties and deformation mechanism of the extruded ZM61 magnesium alloy at high strain rates, *Adv. Eng. Mater.*, 24(2022), No. 8, art. No. 2101554.

[4] S. Abazari, A. Shamsipur, H.R. Bakhsheshi-Rad, *et al*., Carbon nanotubes (CNTs)-reinforced magnesium-based matrix composites: A comprehensive review, *Materials*, 13(2020), No. 19, art. No. 4421.

[5] J.D. Robson and M.R. Barnett, The effect of precipitates on twinning in magnesium alloys, *Adv. Eng. Mater.*, 21(2019), No. 4, art. No. 1800460.

[6] D.R. Lopes, C.L.P. Silva, R.B. Soares, *et al*., Cytotoxicity and corrosion behavior of magnesium and magnesium alloys in hank's solution after processing by high-pressure torsion, *Adv. Eng. Mater.*, 21(2019), No. 8, art. No. 1900391.

[7] Y. Xu, X.X. Zhang, W. Li, *et al*., Mechanical response and microstructure evolution of a repetitive upsetting extrusion processed AZ61 magnesium alloy in semi-solid compression, *Adv. Eng. Mater.*, 21(2019), No. 9, art. No. 1900362.

[8] H.Y. Li, Z.N. Qin, Y.Q. Ouyang, *et al*., Hydroxyapatite/chitosan-metformin composite coating enhances the biocompatibility and osteogenic activity of AZ31 magnesium alloy, *J. Alloys Compd*., 909(2022), art. No. 164694.

[9] Z.K. Gao, W.C. Liu, G.H. Wu, *et al*., Effects of Al and Y addition on microstructures and mechanical properties of as-cast Mg–14Li based alloy, *Adv. Eng. Mater.*, 21(2019), No. 2, art. No.. 1800755.

[10] R. Del Campo, B. Savoini, L. Jordao, A. Muñoz, and M.A. Monge, Cytocompatibility, biofilm assembly and corrosion behavior of Mg–HAP composites processed by extrusion, *Mater. Sci. Eng. C*, 78(2017), p. 667.

[11] M. Rashad, F.S. Pan, J.Y. Zhang, and M. Asif, Use of high energy ball milling to study the role of graphene nanoplatelets and carbon nanotubes reinforced magnesium alloy, *J. Alloys Compd.*, 646(2015), p. 223.

[12] T. Lei, W. Tang, S.H. Cai, F.F. Feng, and N.F. Li, On the corrosion behaviour of newly developed biodegradable Mg-based metal matrix composites produced by *in situ* reaction, *Corros. Sci.*, 54(2012), p. 270.

[13] S. Park, H. Lee, H.E. Kim, H.D. Jung, and T.S. Jang, Bifunctional poly (l-lactic acid)/hydrophobic silica nanocomposite layer coated on magnesium stents for enhancing corrosion resistance and endothelial cell responses, *Mater. Sci. Eng. C*, 127(2021), art. No. 112239.

[14] H. Lee, D.Y. Shin, Y. Na, *et al*., Antibacterial PLA/Mg composite with enhanced mechanical and biological performance for biodegradable orthopedic implants, *Biomater. Adv.*, 152(2023), art. No. 213523.

[15] J.X. Tao, M.C. Zhao, Y.C. Zhao, *et al*., Influence of graphene oxide (GO) on microstructure and biodegradation of $ZK_{30-x}GO$ composites prepared by selective laser melting, *J. Magnesium Alloys*, 8(2020), No. 3, p. 952.

[16] Y.F. Han, Y.B. Ke, Y. Shi, *et al*., Improved mechanical property of nanolaminated graphene (reduced graphene oxide)/Al–Mg–Si composite rendered by facilitated ageing process, *Mater. Sci. Eng. A*, 787(2020), art. No. 139541.

[17] C.J. Shuai, P. Feng, P. Wu, *et al*., A combined nanostructure constructed by graphene and boron nitride nanotubes reinforces ceramic scaffolds, *Chem. Eng. J.*, 313(2017), p. 487.

[18] S. Abazari, A. Shamsipur, H.R. Bakhsheshi-Rad, *et al*., Magnesium-based nanocomposites: A review from mechanical, creep and fatigue properties, *J. Magnesium Alloys*, 11(2023), No. 8, p. 2655.

[19] S. Abazari, A. Shamsipur, H.R. Bakhsheshi-Rad, S. Ramakrishna, and F. Berto, Graphene family nanomaterial reinforced magnesium-based matrix composites for biomedical application: A comprehensive review, *Metals*, 10(2020), No. 8, art. No. 1002.

[20] T. Lei, C. Ouyang, W. Tang, L.F. Li, and L.S. Zhou, Enhanced corrosion protection of MgO coatings on magnesium alloy deposited by an anodic electrodeposition process, *Corros. Sci.*, 52(2010), No. 10, p. 3504.

[21] C.S. Goh, M. Gupta, J. Wei, and L.C. Lee, Characterization of high performance Mg/MgO nanocomposites, *J. Compos. Mater.*, 41(2007), No. 19, p. 2325.

[22] G.Y. Lin, D.D. Liu, M.F. Chen, *et al*., Preparation and characterization of biodegradable Mg–Zn–Ca/MgO nanocomposites for biomedical applications, *Mater. Charact.*, 144(2018), p. 120.

[23] C.J. Shuai, Z.C. Zeng, Y.W. Yang, *et al*., Graphene oxide assists polyvinylidene fluoride scaffold to reconstruct electrical microenvironment of bone tissue, *Mater. Des.*, 190(2020), art. No. 108564.

[24] X.Y. Sun, C.J. Li, X.B. Dai, *et al*., Microstructures and properties of graphene-nanoplatelet-reinforced magnesium-matrix composites fabricated by an *in situ* reaction process, *J. Alloys Compd.*, 835(2020), art. No. 155125.

[25] Y.M. Zhang, J.L. Sun, X.Z. Xiao, N. Wang, G.Z. Meng, and L. Gu, Graphene-like two-dimensional nanosheets-based anticorrosive coatings: A review, *J. Mater. Sci. Technol.*, 129(2022), p. 139.

[26] Z.M. Sun, H.L. Shi, X.S. Hu, M.F. Yan, and X.J. Wang, Simultaneously enhanced mechanical properties and electromagnetic interference shielding performance of a graphene nanosheets (GNSs) reinforced magnesium matrix composite by GNSs induced laminated structure, *J. Alloys Compd.*, 898(2022), art. No. 162847.

[27] V. Berry, Impermeability of graphene and its applications, *Carbon*, 62(2013), p. 1.

[28] H. Wang, C. Wei, K.Y. Zhu, *et al*., Preparation of graphene sheets by electrochemical exfoliation of graphite in confined space and their application in transparent conductive films, *ACS*

Appl. Mater. Interfaces, 9(2017), No. 39, p. 34456.
[29] N. El Mahallawy, A. Ahmed Diaa, M. Akdesir, and H. Palkowski, Effect of Zn addition on the microstructure and mechanical properties of cast, rolled and extruded Mg–6Sn–*x*Zn alloys, *Mater. Sci. Eng. A*, 680(2017), p. 47.
[30] S.C. Tjong, Recent progress in the development and properties of novel metal matrix nanocomposites reinforced with carbon nanotubes and graphene nanosheets, *Mater. Sci. Eng. R Rep.*, 74(2013), No. 10, p. 281.
[31] Z.X. Song, X.S. Hu, Y.Y. Xiang, K. Wu, and X.J. Wang, Enhanced mechanical properties of CNTs/Mg biomimetic laminated composites, *Mater. Sci. Eng. A*, 802(2021), art. No. 140632.
[32] R.F. Albers, R.A. Bini, J.B. Souza, D.T. Machado, and L.C. Varanda, A general one-pot synthetic strategy to reduced graphene oxide (rGO) and rGO-nanoparticle hybrid materials, *Carbon*, 143(2019), p. 73.
[33] A. Bordbar-Khiabani, S. Ebrahimi, and B. Yarmand, Highly corrosion protection properties of plasma electrolytic oxidized titanium using rGO nanosheets, *Appl. Surf. Sci.*, 486(2019), p. 153.
[34] C.D. Gao, P. Feng, S.P. Peng, and C.J. Shuai, Carbon nanotube, graphene and boron nitride nanotube reinforced bioactive ceramics for bone repair, *Acta Biomater.*, 61(2017), p. 1.
[35] M. Rashad, F.S. Pan, A.T. Tang, M. Asif, and M. Aamir, Synergetic effect of graphene nanoplatelets (GNPs) and multi-walled carbon nanotube (MW-CNTs) on mechanical properties of pure magnesium, *J. Alloys Compd.*, 603(2014), p. 111.
[36] M. Rashad, F.S. Pan, A.T. Tang, *et al*., Development of magnesium-graphene nanoplatelets composite, *J. Compos. Mater.*, 49(2015), No. 3, p. 285.
[37] F. Hosseinbabaei and B. Raissidehkordi, Electrophoretic deposition of MgO thick films from an acetone suspension, *J. Eur. Ceram. Soc.*, 20(2000), No. 12, p. 2165.
[38] M.P. Staiger, A.M. Pietak, J. Huadmai, and G. Dias, Magnesium and its alloys as orthopedic biomaterials: A review, *Biomaterials*, 27(2006), No. 9, p. 1728.
[39] C. Blawert, W. Dietzel, E. Ghali, and G. Song, Anodizing treatments for magnesium alloys and their effect on corrosion resistance in various environments, *Adv. Eng. Mater.*, 8(2006), No. 6, p. 511.
[40] S. Petnikota, N.K. Rotte, M.V. Reddy, V.V.S.S. Srikanth, and B.V.R. Chowdari, MgO-decorated few-layered graphene as an anode for Li-ion batteries, *ACS Appl. Mater. Interfaces*, 7(2015), No. 4, p. 2301.
[41] A. Arshad, J. Iqbal, M. Siddiq, *et al*., Graphene nanoplatelets induced tailoring in photocatalytic activity and antibacterial characteristics of MgO/graphene nanoplatelets nanocomposites, *J. Appl. Phys.*, 121(2017), No. 2, art. No. 024901.
[42] C.J. Shuai, B. Wang, S.Z. Bin, S.P. Peng, and C.D. Gao, Interfacial strengthening by reduced graphene oxide coated with MgO in biodegradable Mg composites, *Mater. Des.*, 191(2020), art. No. 108612.
[43] Y. Wang, Z. Fan, X. Zhou, and G.E. Thompson, Characterisation of magnesium oxide and its interface with α-Mg in Mg–Al-based alloys, *Philos. Mag. Lett.*, 91(2011), No. 8, p. 516.
[44] Q.H. Yuan, G.H. Zhou, L. Liao, Y. Liu, and L. Luo, Interfacial structure in AZ91 alloy composites reinforced by graphene nanosheets, *Carbon*, 127(2018), p. 177.
[45] J.T. Hou, W.B. Du, G. Parande, M. Gupta, and S. Li, Significantly enhancing the strength + ductility combination of Mg–9Al alloy using multi-walled carbon nanotubes, *J. Alloys Compd.*, 790(2019), p. 974.
[46] F.P. Du, H. Tang, and D.Y. Huang, Thermal conductivity of epoxy resin reinforced with magnesium oxide coated multi-walled carbon nanotubes, *Int. J. Polym. Sci.*, 2013(2013), art. No. 541823.
[47] F.P. Du, K.B. Wu, Y.K. Yang, L. Liu, T. Gan, and X.L. Xie, Synthesis and electrochemical probing of water-soluble poly(sodium 4-styrenesulfonate-co-acrylic acid)-grafted multiwalled carbon nanotubes, *Nanotechnology*, 19(2008), No. 8, art. No. 085716.
[48] S. Abazari, A. Shamsipur, and H.R. Bakhsheshi-Rad, Reduced graphene oxide (RGO) reinforced Mg biocomposites for use as orthopedic applications: Mechanical properties, cytocompatibility and antibacterial activity, *J. Magnesium Alloys*, 10(2022), No. 12, p. 3612.
[49] X.F. Chen, J.M. Tao, Y.C. Liu, *et al*., Interface interaction and synergistic strengthening behavior in pure copper matrix composites reinforced with functionalized carbon nanotube-graphene hybrids, *Carbon*, 146(2019), p. 736.
[50] C.J. Shuai, B. Wang, Y.W. Yang, S.P. Peng, and C.D. Gao, 3D honeycomb nanostructure-encapsulated magnesium alloys with superior corrosion resistance and mechanical properties, *Composites Part B*, 162(2019), p. 611.
[51] S. Chatterjee, F. Nafezarefi, N.H. Tai, L. Schlagenhauf, F.A. Nüesch, and B.T.T. Chu, Size and synergy effects of nanofiller hybrids including graphene nanoplatelets and carbon nanotubes in mechanical properties of epoxy composites, *Carbon*, 50(2012), No. 15, p. 5380.
[52] Z. Li, G.L. Fan, Q. Guo, Z.Q. Li, Y.S. Su, and D. Zhang, Synergistic strengthening effect of graphene-carbon nanotube hybrid structure in aluminum matrix composites, *Carbon*, 95(2015), p. 419.
[53] C.J. Shuai, Y. Xu, P. Feng, Z.Y. Zhao, and Y.W. Deng, Hybridization of graphene oxide and mesoporous bioactive glass: Micro-space network structure enhance polymer scaffold, *J. Mech. Behav. Biomed. Mater.*, 109(2020), art. No. 103827.
[54] M. Shahin, Munir K., Wen C., and Y.C. Li, Magnesium-based composites reinforced with graphene nanoplatelets as biodegradable implant materials, *J. Alloys Compd.*, 828(2020), art. No. 154461.
[55] C.J. Shuai, T.T. Liu, C.D. Gao, *et al*., Mechanical and structural characterization of diopside scaffolds reinforced with graphene, *J. Alloys Compd.*, 655(2016), p. 86.
[56] H. Hegab, A. Elmekawy, L.D. Zou, D. Mulcahy, C. Saint, and M. Ginic-Markovic, The controversial antibacterial activity of graphene-based materials, *Carbon*, 105(2016), p.362.
[57] Z.J. Jia, Y.Y. Shi, P. Xiong, *et al*., From solution to biointerface: Graphene self-assemblies of varying lateral sizes and surface properties for biofilm control and osteodifferentiation, *ACS Appl. Mater. Interfaces*, 8(2016), No. 27, p. 17151.
[58] M. Torabi Parizi, G.R. Ebrahimi, and H.R. Ezatpour, Effect of graphene nanoplatelets content on the microstructural and mechanical properties of AZ80 magnesium alloy, *Mater. Sci. Eng. A*, 742(2019), p. 373.
[59] M. Torabi Parizi, H.R. Ezatpour, and G.R. Ebrahimi, High mechanical efficiency, microstructure evaluation and texture of rheo-casted and extruded AZ80–Ca alloy reinforced with processed Al_2O_3/GNPs hybrid reinforcement, *Mater. Chem. Phys.*, 218(2018), p. 246.
[60] K.S. Munir, Y.C. Li, J.X. Lin, and C.E. Wen, Interdependencies between graphitization of carbon nanotubes and strengthening mechanisms in titanium matrix composites, *Materialia*, 3(2018), p. 122.
[61] M. Wang, Y. Zhao, L.D. Wang, *et al*., Achieving high strength and ductility in graphene/magnesium composite via an *in situ* reaction wetting process, *Carbon*, 139(2018), p. 954.
[62] C.J. Shuai, B. Wang, S.Z. Bin, S.P. Peng, and C.D. Gao, TiO_2-induced *in situ* reaction in graphene oxide-reinforced AZ61 biocomposites to enhance the interfacial bonding, *ACS Appl. Mater. Interfaces*, 12(2020), No. 20, p. 23464.
[63] P. Nyanor, O. El-Kady, H.M. Yehia, A.S. Hamada, K. Nakamura, and M.A. Hassan, Effect of carbon nanotube (CNT) content on the hardness, wear resistance and thermal expansion of *In-situ* reduced graphene oxide (rGO)-reinforced aluminum matrix composites, *Met. Mater. Int.*, 27(2021), No. 5, p. 1315.
[64] J.F. Wang, W.W. Wei, X.F. Huang, L. Li, and F.S. Pan, Prepar-

ation and properties of Mg–Cu–Mn–Zn–Y damping magnesium alloy, *Mater. Sci. Eng. A*, 528(2011), No. 21, p. 6484.
[65] C.J. Shuai, J. Zan, F.W. Qi, *et al*., nMgO-incorporated PLLA bone scaffolds: Enhanced crystallinity and neutralized acidic products, *Mater. Des.*, 174(2019), art. No. 107801.
[66] Y.P. Ding, J.L. Xu, J.B. Hu, *et al*., High performance carbon nanotube-reinforced magnesium nanocomposite, *Mater. Sci. Eng. A*, 771(2020), art. No. 138575.
[67] P.B. Wang, J. Shen, T.J. Chen, Q.L. Li, X.A. Yue, and L.Y. Wang, Fabrication of graphene nanoplatelets reinforced Mg matrix composites via powder thixoforging, *J. Magnesium. Alloys*, 10(2022), No. 11, p. 3113.
[68] Q.H. Yuan, X.S. Zeng, Y. Liu, *et al*., Microstructure and mechanical properties of AZ91 alloy reinforced by carbon nanotubes coated with MgO, *Carbon*, 96(2016), p. 843.
[69] S.L. Xiang, X.J. Wang, M. Gupta, K. Wu, X.S. Hu, and M.Y. Zheng, Graphene nanoplatelets induced heterogeneous bimodal structural magnesium matrix composites with enhanced mechanical properties, *Sci. Rep.*, 6(2016), art. No. 38824.
[70] X. Du, W.B. Du, Z.H. Wang, K. Liu, and S.B. Li, Ultra-high strengthening efficiency of graphene nanoplatelets reinforced magnesium matrix composites, *Mater. Sci. Eng. A*, 711(2018), p. 633.
[71] S. Ramezanzade, G.R. Ebrahimi, M. Torabi Parizi, and H.R. Ezatpour, Synergetic effect of GNPs and MgOs on the mechanical properties of Mg–Sr–Ca alloy, *Mater. Sci. Eng. A*, 761(2019), art. No. 138025.
[72] L. Zhang, W.W. Liu, C.G. Yue, *et al*., A tough graphene nanosheet/hydroxyapatite composite with improved *in vitro* biocompatibility, *Carbon*, 61(2013), p. 105.
[73] Y.Y. Shi, M. Li, Q. Liu, *et al*., Electrophoretic deposition of graphene oxide reinforced chitosan-hydroxyapatite nanocomposite coatings on Ti substrate, *J. Mater. Sci. Mater. Med.*, 27(2016), No. 3, art. No. 48.
[74] F. Gao, C.Y. Xu, H.T. Hu, *et al*., Biomimetic synthesis and characterization of hydroxyapatite/graphene oxide hybrid coating on Mg alloy with enhanced corrosion resistance, *Mater. Lett.*, 138(2015), p. 25.
[75] X.H. Sun, X. Yu, W. Li, M.F. Chen, and D.B. Liu, Mechanical properties, degradation behavior and cytocompatibility of biodegradable 3vol%X (X = MgO, ZnO and CuO)/Zn matrix composites with excellent dispersion property fabricated by graphene oxide-assisted hetero-aggregation, *Biomater. Adv.*, 134(2022), art. No. 112722.
[76] N. Safari, N. Golafshan, M. Kharaziha, *et al*., Stable and antibacterial magnesium–graphene nanocomposite-based implants for bone repair, *ACS Biomater. Sci. Eng.*, 6(2020), No. 11, p. 6253.
[77] T.S.N. Sankara Narayanan, I.S. Park, and M.H. Lee, Strategies to improve the corrosion resistance of microarc oxidation (MAO) coated magnesium alloys for degradable implants: Prospects and challenges, *Prog. Mater. Sci.*, 60(2014), p. 1.
[78] M.E. Orazem, N. Pébère, and B. Tribollet, Enhanced graphical representation of electrochemical impedance data, *J. Electrochem. Soc.*, 153(2006), No. 4, art. No. B129.
[79] W.C. Kim, J.G. Kim, J.Y. Lee, and H.K. Seok, Influence of Ca on the corrosion properties of magnesium for biomaterials, *Mater. Lett.*, 62(2008), No. 25, p. 4146.
[80] G. Jena, B. Anandkumar, S.C. Vanithakumari, R.P. George, J. Philip, and G. Amarendra, Graphene oxide–chitosan–silver composite coating on Cu–Ni alloy with enhanced anticorrosive and antibacterial properties suitable for marine applications, *Prog. Org. Coat.*, 139(2020), art. No. 105444.
[81] B.K. Jiang, A.Y. Chen, J.F. Gu, *et al*., Corrosion resistance enhancement of magnesium alloy by N-doped graphene quantum dots and polymethyltrimethoxysilane composite coating, *Carbon*, 157(2020), p. 537.
[82] P. Feng, P. Wu, C.D. Gao, *et al*., A multimaterial scaffold with tunable properties: Toward bone tissue repair, *Adv. Sci.*, 5(2018), No. 6, art. No. 1700817.
[83] H.R. Bakhsheshi-Rad, A.F. Ismail, M. Aziz, *et al*., Co-incorporation of graphene oxide/silver nanoparticle into poly-L-lactic acid fibrous: A route toward the development of cytocompatible and antibacterial coating layer on magnesium implants, *Mater. Sci. Eng. C*, 111(2020), art. No. 110812.
[84] S. Panda, T.K. Rout, A.D. Prusty, P.M. Ajayan, and S. Nayak, Electron transfer directed antibacterial properties of graphene oxide on metals, *Adv. Mater.*, 30(2018), No. 7, art. No. 1702149.
[85] G.W. Qian, L.M. Zhang, Y. Shuai, *et al*., 3D-printed $CuFe_2O_4$–MXene/PLLA antibacterial tracheal scaffold against implantation-associated infection, *Appl. Surf. Sci.*, 614(2022), No. 3, art. No.156108.
[86] S. Abazari, A. Shamsipur, and H.R. Bakhsheshi-Rad, Synergistic effect of hybrid reduced graphene oxide (rGO) and carbon nanotubes (CNTs) reinforcement on microstructure, mechanical and biological properties of magnesium-based composite, *Mater. Chem. Phys.*, 301(2023), art. No. 127543.
[87] S. Liu, T.H. Zeng, M. Hofmann, *et al*., Antibacterial activity of graphite, graphite oxide, graphene oxide, and reduced graphene oxide: Membrane and oxidative stress, *ACS Nano*, 5(2011), No. 9, p. 6971.
[88] X.F. Zou, L. Zhang, Z.J. Wang, and Y. Luo, Mechanisms of the antimicrobial activities of graphene materials, *J. Am. Chem. Soc.*, 138(2016), No. 7, p. 2064.
[89] J. Zhao, Z.Y. Wang, J.C. White, and B.S. Xing, Graphene in the aquatic environment: Adsorption, dispersion, toxicity and transformation, *Environ. Sci. Technol.*, 48(2014), No. 17, p. 9995.
[90] S.B. Liu, L. Wei, L. Hao, *et al*., Sharper and faster "nano darts" kill more bacteria: A study of antibacterial activity of individually dispersed pristine single-walled carbon nanotube, *ACS Nano*, 3(2009), No. 12, p. 3891.
[91] D. Wang, C. Ma, J.Y. Liu, *et al*., Corrosion resistance and antisoiling performance of micro-arc oxidation/graphene oxide/stearic acid superhydrophobic composite coating on magnesium alloys, *Int. J. Miner. Metall. Mater.*, 30(2023), No. 6, p. 1128.
[92] M. Razzaghi, M. Kasiri-Asgarani, H.R. Bakhsheshi-Rad, and H. Ghayour, *In vitro* bioactivity and corrosion of PLGA/hardystonite composite-coated magnesium-based nanocomposite for implant applications, *Int. J. Miner. Metall. Mater.*, 28(2021), No. 1, p. 168.
[93] H. Mirzadeh, Surface metal-matrix composites based on AZ91 magnesium alloy via friction stir processing: A review, *Int. J. Miner. Metall. Mater.*, 30(2023), No. 7, p. 1278.
[94] J.L. Su, J. Teng, Z.L. Xu, and Y. Li, Biodegradable magnesium-matrix composites: A review, *Int. J. Miner. Metall. Mater.*, 27(2020), No. 6, p. 724.
[95] S. Jabbarzare, H.R. Bakhsheshi-Rad, A.A. Nourbakhsh, T. Ahmadi, and F. Berto, Effect of graphene oxide on the corrosion, mechanical and biological properties of Mg-based nanocomposite, *Int. J. Miner. Metall. Mater.*, 29(2022), No. 2, p. 305.
[96] Z.D. Wang, K.B. Nie, K.K. Deng, and J.G. Han, Effect of extrusion on the microstructure and mechanical properties of a low-alloyed Mg−2Zn−0.8Sr−0.2Ca matrix composite reinforced by TiC nano-particles, *Int. J. Miner. Metall. Mater.*, 29(2022), No. 11, p. 1981.